Hydrodynamic structures of droplets in square micro-channels

Flavie Sarrazin[2,4], Thomas Bonometti[3], Laurent Prat[1,2], Christophe Gourdon[1,2], Jacques Magnaudet[3]

[1] Université de Toulouse, INPT-ENSIACET, 5 rue Paulin Talabot, Paulin, 31106 Toulouse Cedex 1, France
[2] Laboratoire de Génie Chimique de Toulouse (LGC), UMR CNRS/INPT/UPS 5503, France
[3] Institut de Mécanique des Fluides de Toulouse (IMFT), UMR CNRS/INPT/UPS 5502, France
[4] Laboratoire du Futur (LOF), UMR RHODIA/CNRS/BORDEAUX I 5258, France.

Abstract

This paper reports on numerical simulations of the hydrodynamics inside droplets in rectangular micro-channels. We use a finite-volume/front-capturing method that allows us to perform two- and three-dimensional simulations with a reasonable cost. The numerical method is an interface-capturing technique without any interface reconstruction. Therefore no complex or expensive interface tracking is needed. Droplet interface deformation and velocity fields inside both droplets and continuous phase can then be followed. This study leads to important results about droplet deformation and inner streamlines for mass and heat transfer studies. More particularly, the capillary number seems to have a great influence on the liquid/liquid flow hydrodynamics whatever is the channel width.

1. Introduction

One of the determining objectives for Fine Chemistry or Pharmaceutical industries is to improve the initial step of physical and chemical data acquisition. For fast process development, a very promising application of two-phase flow in microchannels is to use micro droplets as individual nano-volume batch reactors. These devices can be focused on determining chemical stoechiokinetics (Song et al., 2003, Sarrazin et al., 2007) and mass and heat transfer parameters (Dummann et al., 2003 ; Burns and Ramshaw, 2001).

In order to choose the correct geometry and the operating parameters of such systems, first preliminary study must be done by using global dimensionless numbers, directly measurable by the operator (such as channel dimension, droplet velocity and shape…). The necessary information lies then in the link between these global characterizations and the local behavior of the phases accessible through numerical simulations.

Several studies focused on simulating two-phase flows inside milli and micro channels. Harries *et al*. (2003) used a CFD code to investigate the internal flow patterns of fluid segmented flows in a microreactor and the transfer of dissolved species within the segments and across the interfaces. Their simulation was two-dimensional and the segment was assumed to have a rectangular shape. Kashid *et al*. (2005) studied the internal circulation within liquid slugs of a liquid-liquid microreactor. They performed two-dimensional computations using a CFD particle tracing algorithm. Stone and Stone (2005) imaged and quantified mixing in a micromixer: their model consists in a spherical droplet immersed in a periodic sequence of distinct external flows, which are superposition of uniform and shear

flows. The purpose is to investigate stirring in three-dimensional systems. Muradoglu and Stone (2005) used a Front Tracking method to simulate advective effects inside a two-dimensional droplet circulating in a serpentine channel. The droplet shape is calculated self-consistently, molecular mixing is ignored, and only mixing by chaotic advection is considered. The effect of dimensionless parameters such as the capillary number, the Reynolds number, the relative droplet radius and the viscosity ratio were investigated.

This paper reports on numerical simulations of the hydrodynamics inside droplets in rectangular micro-channels. We use a finite-volume/front-capturing method that allows us to perform two- and three-dimensional simulations with a reasonable cost. The numerical method is an interface-capturing technique without any interface reconstruction. Therefore no complex or expensive interface tracking is needed. The code has been experimentally validated in previous work thanks to micro-PIV (Sarrazin *et al*., 2006).
Droplet interface deformation and velocity fields inside both droplets and continuous phase can then be followed. These results allow linking global and local characteristics of the droplets.

2. Direct numerical simulations

2.1. Numerical method

The numerical method is an interface-capturing technique that does not use any interface reconstruction. We assume the two fluids to be Newtonian and incompressible, with uniform surface tension and no phase change. The evolution of the two-phase flow is then classically described using the one-fluid formulation of the Navier-Stokes equations, namely:

$$\frac{\partial \boldsymbol{U}}{\partial t} + \boldsymbol{U}.\nabla \boldsymbol{U} = -\frac{1}{\rho}\nabla P + \boldsymbol{g} + \frac{1}{\rho}\nabla \cdot \left[\mu\left(\nabla \boldsymbol{U} + {}^{t}\nabla \boldsymbol{U}\right)\right] - \frac{\sigma}{\rho}(\nabla.\boldsymbol{n})\boldsymbol{n}\delta_I \;;\; \nabla \cdot \boldsymbol{U} = 0 \;, \quad (1)$$

where $\boldsymbol{U}$, P, ρ and μ are the local velocity, pressure, density and dynamical viscosity in the flow, respectively, $\boldsymbol{g}$ denotes gravity and σ is the surface tension. The surface delta function δ_I is zero outside the interface, the unit normal of which (directed toward the continuous phase) is denoted by $\boldsymbol{n}$. The local volume fraction of fluid 1 obeys:

$$\frac{\partial C}{\partial t} + \boldsymbol{U}.\nabla C = 0 \;. \quad (2)$$

This volume fraction equals one (resp. zero) in cells filled with fluid 1 (resp. 2) and takes intermediate values in cells belonging to the transition region. The local density and dynamical viscosity are evaluated using a linear interpolation, namely:

$$\rho = C\rho_1 + (1-C)\rho_2 \quad ; \quad \mu = C\mu_1 + (1-C)\mu_2 \,. \quad (3)$$

The capillary force is transformed into a volume force using the Continuum Surface Force model proposed by Brackbill et al (1992). Hence we write:

$$\frac{\sigma}{\rho}(\nabla.\boldsymbol{n})\boldsymbol{n}\delta_I = \frac{\sigma}{\rho}\nabla.\left(\frac{\nabla C}{\|\nabla C\|}\right)\nabla C \;. \quad (4)$$

The Navier-Stokes equations (1) are solved using the JADIM code developed at IMFT. Details on the spatial discretization and time-advancement algorithm used in this code for

constant density situations may be found in several previous publications (Magnaudet *et al*., 1995; Calmet and Magnaudet, 1997; Legendre and Magnaudet, 1998). Briefly, the momentum equations are discretized on a staggered orthogonal grid using a finite-volume approach. The spatial discretization is performed using second-order centered differences. Time-advancement is achieved through a third-order Runge-Kutta method for advective and source terms and a Crank-Nicholson method for viscous stresses. Incompressibility is satisfied at the end of each time step through a projection method. The overall algorithm is second-order accurate in both time and space.
To solve Eq. (2), we split it into successive one-dimensional steps along each grid direction i (i=1,3) and use a Flux Corrected Transport scheme (Zalesak, 1979) for each substep. To prevent the transition region $0<C<1$ from thickening as time proceeds we make the velocity field involved in (2) locally constant across it. This procedure allows us to keep the thickness of the transition region within three cells. Further details about the transport of the volume fraction may be found in Bonometti and Magnaudet, 2006.

To understand the driving effects in such flows, the capillary number Ca, the Weber number We and the Bond number Bo are evaluated. Considering an equivalent diameter $D_{eq}=1.33D$, a droplet velocity U_d=0.05 m/s and taking into account the physical properties of the continuous phase (the viscosity μ=20 cp and the density ρ=980 kg.m^{-3}), we obtain $Ca=\mu_c U_d/\sigma = 0.1$, $We = \rho_c U_d^2 D_{eq}/\sigma = 2.10^{-2}$, $Bo = |\rho_c-\rho_d| g D_{eq}^2/\sigma = 3.10^{-4}$ (g denotes gravity) and $Re_d=\rho_c U_d D_{eq}/\mu_c=0.19$. Thus the leading effects are in decreasing order, surface tension, viscosity, inertia and gravity, respectively.

As gravity has no effect on the flow, we assume the latter to be symmetric along the vertical and horizontal middle planes. In addition, the configuration of the droplet chain is reduced to the study of a single droplet by applying periodic conditions at the boundaries normal to the mean flow direction. The computational dimensions and the grid size are plotted in Figure 1. Free-slip conditions are imposed on boundaries corresponding to the droplet symmetry planes; the other boundaries parallel to the mean flow direction are considered as rigid walls. The grid is refined near the walls in order to capture accurately the hydrodynamics of the liquid film separating the droplets from the walls (see Figure 1).

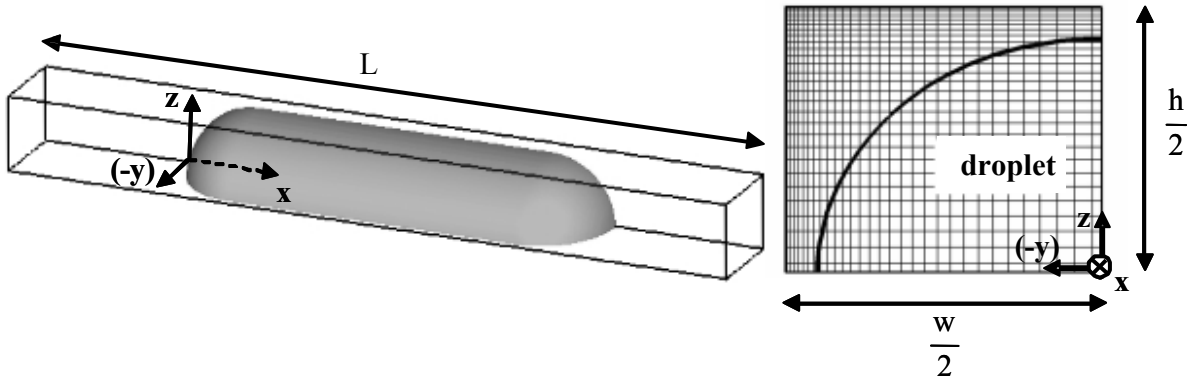

Figure 1: (a) Computational domain and initial drop shape; (b) detail of the grid over one quarter of the channel (thick line indicates the initial position of the drop)

2.2. Operating conditions and measurements

In the studied cases, the dispersed phase is water and the continuous phase corresponds to a silicon oil (the viscosity μ=20 cp and the density ρ=980 kg.m^{-3}). Two different surface tensions have been used: σ=0.01 mN.m^{-1} and σ=0.038 mN.m^{-1}. The channel dimension w varies from 50 to 960 µm. Droplets sizes are characterized by their width and a shape factor defined as: α=*length/width* which varies from 1 to 8. Finally, the droplet velocities lie between 0.01 and 0.2 m.s^{-1}.

The simulations are characterised by the droplets velocity U_d (m.s^{-1}), the continuous phase velocity U_c (m.s^{-1}) and a slip coefficient β:

$$U_d = \frac{\int_0^L \int_0^{\frac{w}{2}} \int_0^{\frac{h}{2}} C \cdot (U \cdot n) \cdot dxdydz}{\int_0^L \int_0^{\frac{w}{2}} \int_0^{\frac{h}{2}} C \cdot dxdydz} \quad ; \quad U_c = \frac{\int_0^L \int_0^{\frac{w}{2}} \int_0^{\frac{h}{2}} (1-C) \cdot (\mathbf{U} \cdot \mathbf{n}) \cdot dxdydz}{\int_0^L \int_0^{\frac{w}{2}} \int_0^{\frac{h}{2}} (1-C) \cdot dxdydz} \quad ; \quad \beta = \frac{U_d - U_c}{U_d} \qquad (5)$$

Furthermore, the interface position (between the channel centre and the interface) is measured and normalized by half the channel width: (y_i). A characteristic time of the system T^*_{loop} is also calculated:

$$T^*_{loop} = \frac{T_{loop}}{T_{convection}} \qquad (6)$$

where T_{loop} is the recirculation time of one loop inside the droplet and $T_{convection}$ is the time for one droplet to cross its own length. The confinement of the droplet is important.

3. Results and discussion

3.1. Three-dimensional structures

Two droplets hydrodynamics are simulated in the same conditions of grid, initial volume and pressure drop. Physical properties are the same for both cases, except the surface tension (0.038 N.m^{-1} for case 1 and 0.01 N.m^{-1} for case 2). Channel is 50×60µm in size. Results are presented in Figure 2 and some global measurements reported in Table 1.

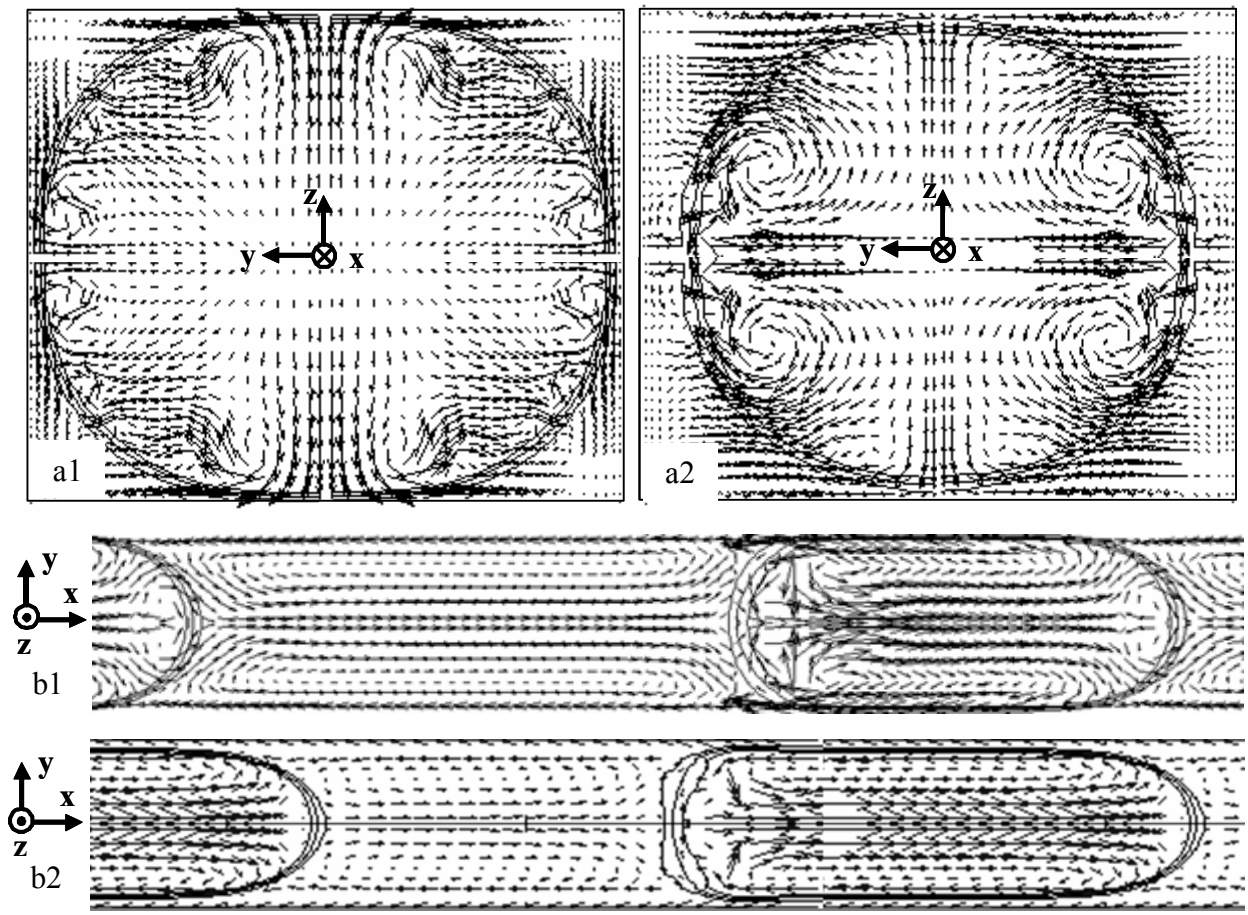

Figure 2: 3D simulations case 1 (σ = 0.038 mN.m^{-1}) and case 2 (σ = 0.010 mN.m^{-1}) : (a) transversal section of the channel at the middle of droplet ; (b) results in the direction of the flow at the quarter of droplet. Interface is represented by isovalues of continuous phase volume fraction (0.05; 0.5; 0.95), showing the robustness of the numerical method (low dispersion of the interface after 280000 iterations).

Case	σ (mN.m^{-1})	Droplet velocity (m.s^{-1})	Re	Ca	β (%)	y_i
1	0.038	0.044	0.13	0.022	33	0.96
2	0.01	0.083	0.25	0.157	57	0.84

Table 1: global measurements and characteristics of the simulations.

In case 1, the liquid film between droplet and wall is smaller and the droplet interface tends to follow the channel shape. Compared to case 2, droplet velocity is smaller as the friction is more important. The continuous phase mainly flows in the angles of the channel and the slip velocity is smaller. Finally, in case 1, the recirculation loop at the front of the droplet is more important than in case 2.

In case 2, the capillary number is higher. The transversal section is quite circular. To maintain this shape, an important internal recirculation loop has developed from the wall to the center of the drop. The continuous phase film at the wall is more important than in case 1. Then the droplet is more stretched and the flow in the film is important, increasing the slip velocity.

3.2. Influence of confinement

Figure 3 (a, b and c) shows the internal droplets behaviour function of the simulation conditions (reported in Table 2) in order to characterize the influence of the confinement. When the droplet is too much contained (case a), a quite static zone appears around the recirculation node. In such a case, compared to the convection time, the dimensionless loop time is the highest. With a shape factor slightly different (case b), the recirculation are more centred on the node and the static zone is then less important. The contact between droplet and the channel walls is still enough important to insure a good contribution of the convection.
When the channel size increases (case c), the droplet tends to a sphere. As the interface moves away from the walls, the internal velocity of the loops decreases in intensity. Furthermore, there is no recirculation at the back of the droplets (as observed by Amar *et al*., 2005).

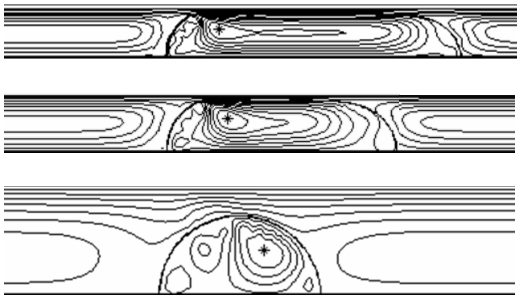

Figure 3: stream lines in droplet referential.
Influence of confinement for same droplet volume.

Case	w (μm)	σ (μN.m^{-1})	Droplet velocity (m.s^{-1})	Re	Ca	β (%)	y_i	T^*_{loop}
a	50	0.038	0.05	0.011	0.03	19	0.9	3.56
b	60	0.038	0.034	0.011	0.02	13	0.91	3.08
c	120	0.038	0.016	0.011	0.01	6	0.67	2.01

Table 2: global measurements and characteristics of the simulations.

3.3. Influence of the shape factor

Figure 4 (d, e and f) shows the internal droplets behaviour function of the simulation conditions (reported in Table 3) in order to characterize the influence of the shape factor. The internal loop time increases logically with the increase of the droplet length. But there is an optimum in term of dimensionless loop time. Indeed, for high values of α, the recirculation loop follows the droplet shape. This implies a more important static zone around the node (where the internal loops velocities are smaller). On the contrary, for low values of α, the contact with the walls is reduced and the slip velocity more important. This implies a reduction of the internal droplet velocity gradient and then a reduction of the convection impact.
This optimum in behaviour is dependent of the surface tension. Indeed, as shown previously, a decrease in the Capillary number enhances the apparition of a secondary loop and a more important velocity gradient. In such a case, the static zone around the node decreases.

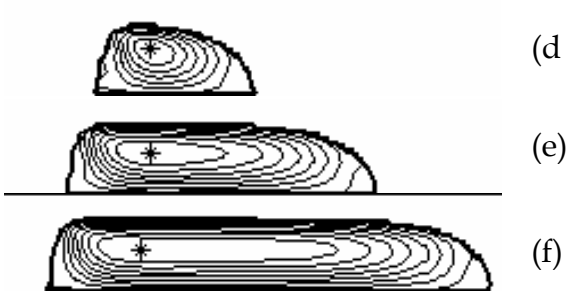

Figure 4: stream lines in droplet referential.
Influence of shape factor for same channel size.

Case	w (μm)	σ (μN.m^{-1})	Droplet velocity (m.s^{-1})	Re	Ca	β (%)	y_i	T^*_{loop}
d	60	0.01	0.133	0.28	0.25	28	0.85	4.04
e	60	0.01	0.150	0.33	0.29	32	0.73	3.61
f	60	0.01	0.131	0.29	0.25	36	0.73	3.94

Table 3: global measurements and characteristics of the simulations.

3.4. Influence of channel size

Figure 5 (g, h and i) shows the internal droplets behaviour function of the simulation conditions (reported in Table 4) in order to characterize the influence of the channel size. A secondary recirculation loop appears at the front of the droplet when the velocity decreases or when the channel size increases (for low *Re* or *Ca* numbers). This has been previously observed and described (in Sarrazin *et al*., 2006). This secondary loop moves the recirculation node to the back of the droplet and its rotation characteristic time is smaller than the one of the main loop.

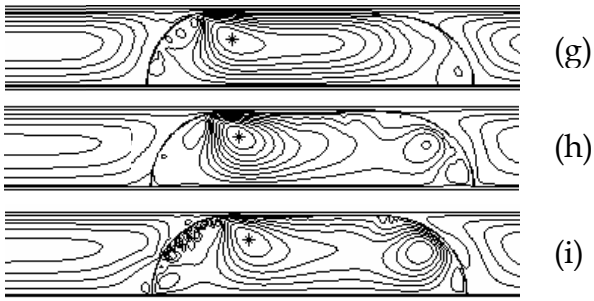

Figure5: stream lines in droplet referential.
Influence of channel size for same shape factor.

Case	w (μm)	σ (μN.m^{-1})	Droplet velocity (m.s^{-1})	Re	Ca	β (%)	y_i	T^*_{loop}
g	60	0.038	0.04	0.11	0.02	16	0.91	2.91
h	60	0.038	0.0095	0.03	0.005	13	0.93	1.16
i	480	0.038	0.0036	0.09	0.002	7	0.96	1.86

Table 4: global measurements and characteristics of the simulations.

3.6. Interface and recirculation node positions

Interface and recirculation node positions are measured for all the previously described experiments and represented versus *Ca* number in Figure 6. For low values of *Ca*, the interface position is quite constant around 90 % of the channel size and the node position constant around 65 % of the channel size. When *Ca* goes over 0.04, the film thickens and the node approaches the interface. Such behaviors have been described for gas-liquid systems (Thulasidas *et al*., 1997). Furthermore, the relative thickness of the film compared to the channel dimension and the slip ratio are directly linked to *Ca*. This is shown on figure 7. The relative film thickness and the slip coefficient β increase in $Ca^{1/3}$.

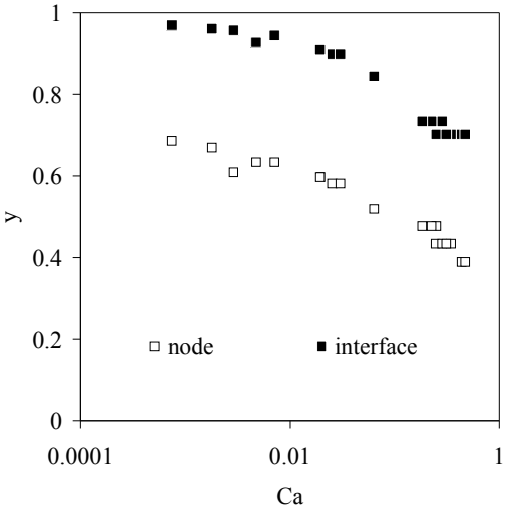

Figure 6: influence of the Capillary number on the description of the hydrodynamic structures (node and interface positions).

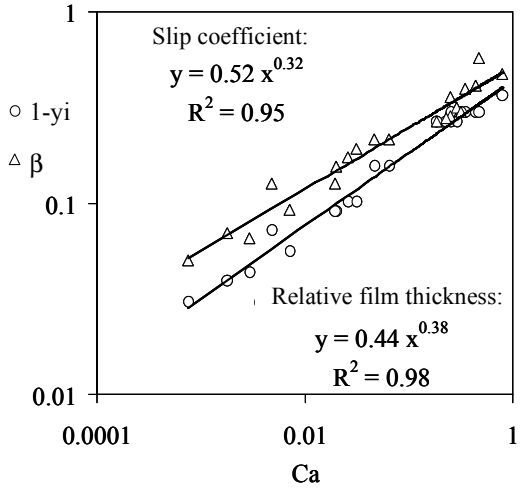

Figure 7: slip ratio and relative film thickness versus Capillary number.

The main interest in working in square or rectangular section channels lies in the presence of a leakage flow in the angles of the channel. This reduces the slip velocity between the two phases. A high velocity gradient is then preserved inside the droplets, enhancing the contribution of convection on the internal phenomena such as mass or heat transfer.

4. Conclusion

The hydrodynamic of droplets moving in square micro channels is studied by direct simulation. Several parameters are varied such as the velocity, the shape factor, the dimension of the channel or the surface tension. The internal hydrodynamic structures developed in the droplets are characterized by the position of the static node, the position of the film and the presence of a secondary recirculation loop.

The confinement influences drastically the internal droplets structures. The contact with the channel walls increases the impact of the convection and the apparition of internal recirculation loops. Finally a direct correlation between the capillary number and the structures is proposed.

References

Amar A., Stapf S. and Blümich B. (2005) Internal fluid dynamics in levitated drops by fast magnetic resonance velocimetry, Physical Review E. 72, 030201.

Bonometti T. and Magnaudet J. (2006) Transition from spherical cap to toroidal bubbles. Phys. Fluids. 18, 052102.

Brackbill JU, Kothe DB, Zemach C. (1992) A continuum method for modeling surface tension. J. Comput. Phys.; 100, 335-354.

Burns J.R. and Ramshaw C. The intensification of rapid reactions in multiphase systems using slug flow in capillaries. Lab Chip; 2001; 1, 10-15.

Calmet I, Magnaudet J. (1997), Large eddy simulation of high-Schmidt-number mass transfer in a turbulent channel flow. Phys. Fluids.; 9, 438-455.

Dummann G., Quittmann U., Gröschel L., Agar D.W., Wörz O. and Morgenchweiss K. (2003) The capillary-microreactor: a new reactor concept for the intensification of heat and mass transfer in liquid-liquid reactions. Catalysis Today; 79-80, 433-439.

Harries N, Burns JR, Barrow DA. (2003) A numerical model for segmented flow in a microreactor. Int. J. Heat Mass Tran.; 46 (17), 3313-3322.

Kashid MN, Gerlach I, Goetz S. (2005) Internal circulation within the liquid slugs of a liquid-liquid slug-flow capillary microreactor. Ind. End. Chem. Res.; 44 (14), 5003-5010.

Legendre D, Magnaudet J. (1998), The lift force on a spherical bubble in a viscous linear shear flow. J. Fluid Mech.; 368, 81-126.

Magnaudet J, Rivero M, Fabre J. (1995), Accelerated flows around a rigid sphere or a spherical bubble. Part I: Steady straining flow. J. Fluid Mech. 1995; 284, 97-135.

Muradoglu M, Stone HA. (2005) Mixing in a drop moving through a serpentine channel: A computational study. Phys. Fluids.; 17, 073305.

Sarrazin F., Bonometti T., Loubière K., Prat L., Gourdon C., Magnaudet J. (2006) Experimental and numerical study of droplets hydrodynamics in microchannels, AIChE, 52 (12), p4061-4070.

Sarrazin F., Prat L., Di Miceli N., Cristobal G., Link D.R. and Weitz D.A. (2007) Mixing characterization inside micro-droplets engineered on a microcoalescer, Chemical Engineering Science, 62 (4), p1042-1048.

Song, H., Tice J.D. and Ismagilov R. (2003) A microfluidics system for controlling reaction networks in time. Angew. Chem. Int. Ed.; 42, 768-771.

Stone ZB, Stone HA. (2005) Imaging and quantifying mixing in a model droplet micromixer. Phys. Fluids.; 17 (6), 063103.

Thulasidas T.C., Abraham M.A. and Cerro R.L. (1997), “Flow patterns in liquid slugs during bubble trains flow inside capillaries”, Chemical Engineering Science, 52, n° 17, 2947-2962.

Zalesak ST. (1979) Fully multidimensional Flux-Corrected Transport algorithms for fluids. J. Comput. Phys.; 31, 335-362.